

Brain aging, cognition in youth and old age and vascular disease in the Lothian Birth Cohort 1936: rationale, design and methodology of the imaging protocol*

Joanna M. Wardlaw^{1,2,3,†}, Mark E. Bastin^{1,2,3,4,†}, Maria C. Valdés Hernández^{1,2,3}, Susana Muñoz Maniega^{1,2,3}, Natalie A. Royle^{1,2,3}, Zoe Morris^{1,2}, Jonathan D. Clayden⁵, Elaine M. Sandeman^{1,2}, Elizabeth Eadie⁶, Catherine Murray^{3,7}, John M. Starr^{3,8}, and Ian J. Deary^{3,7}

Rationale As the population of the world ages, age-related cognitive decline is becoming an ever-increasing problem. However, the changes in brain structure that accompany normal aging, and the role they play in cognitive decline, remain to be fully elucidated.

Aims This study aims to characterize changes in brain structure in old age, and to investigate relationships between brain aging and cognitive decline using the Lothian Birth Cohort 1936. Here, we report the rationale, design and methodology of the brain and neurovascular imaging protocol developed to study this cohort.

Design An observational, longitudinal study of the Lothian Birth Cohort 1936, which comprises 1091 relatively healthy individuals now in their 70s and living in the Edinburgh area. They are surviving participants of the Scottish Mental Survey 1947, which involved a test of general intelligence taken at age 11 years. At age 70 years, the Lothian Birth Cohort 1936 undertook detailed cognitive, medical and genetic testing, and provided social, family, nutritional, quality of life and

physical activity information. At mean age 73 years they underwent detailed brain MRI and neurovascular ultrasound imaging, repeat cognitive and other testing. The MRI protocol is designed to provide qualitative and quantitative measures of gray and white matter atrophy, severity and location of white matter lesions, enlarged perivascular spaces, brain mineral deposits, microbleeds and integrity of major white matter tracts. The neurovascular ultrasound imaging provides velocity, stenosis and intima-media thickness measurements of the carotid and vertebral arteries.

Study This valuable imaging dataset will be used to determine which changes in brain structural parameters have the largest effects on cognitive aging. Analysis will include multi-modal image analysis and multivariate techniques, such as factor analysis and structural equation modelling. Especially valuable is the ability within this sample to examine the influence that early life intelligence has on brain structural parameters in old age, and the role of genetic, vascular, educational and lifestyle factors.

Outcomes Final outcomes include associations between early and late life cognition and integrity of key white matter tracts, volume of gray and white matter, myelination, brain water content, and visible abnormalities such as white matter lesions and mineral deposits; and influences of vascular risk factors, diet, environment, social metrics, education and genetics on healthy brain aging. It is intended that this information will help to inform and develop strategies for successful cognitive aging.

Key words: brain, MRI, Normal ageing

Correspondence: J. M. Wardlaw*, Brain Research Imaging Centre, Division of Clinical Neurosciences, University of Edinburgh, Western General Hospital, Crewe Road, Edinburgh EH4 2XU, UK
E-mail: joanna.wardlaw@ed.ac.uk

¹Brain Research Imaging Centre, Division of Clinical Neurosciences, University of Edinburgh, Edinburgh, UK

²Scottish Imaging Network, A Platform for Scientific Excellence (SINAPSE) Collaboration, Edinburgh, UK

³Centre for Cognitive Ageing and Cognitive Epidemiology (CCACE), University of Edinburgh, Edinburgh, UK

⁴Health Sciences (Medical Physics), University of Edinburgh, Edinburgh, UK

⁵Institute of Child Health, University College London, London, UK

⁶Department of Neuroradiology, Western General Hospital, NHS Lothian, Edinburgh, UK

⁷Department of Psychology, University of Edinburgh, Edinburgh, UK

⁸Geriatric Medicine Unit, University of Edinburgh, Edinburgh, UK

*Conflicts of interest: None declared.

†Contributed equally.

DOI: 10.1111/j.1747-4949.2011.00683.x

Introduction

Some important domains of cognitive ability, such as memory, reasoning and processing speed, decline with advancing age (1). Those who experience relatively greater levels of decline are more likely to have less independence and a lower quality of life. Aging is also associated with vascular and Alzheimer's

dementias, although there is evidence that early life mental ability may help protect against dementia (2). With the world facing an aging demographic, strategies to preserve cognitive and physiological functions and prevent age-related diseases are of government priority in many countries (3); early cognitive decline is a stage where intervention is most likely to be effective. The biological basis of cognitive ability and how it changes with age is therefore of enormous interest (4). In particular, the biological basis of cognitive reserve, of which childhood mental ability is a useful index (5), is important in any life course approach to cognitive aging.

Although there is considerable variation between individuals, both gray and white matter is gradually lost in normal aging, with rapid tissue loss often presaging dementia (6). While the focus of much recent imaging research has been on the cortex, it is clear that substantial white matter damage also occurs (7). White matter fibers connect different cortical regions together underpinning brain function. Age-related damage to white matter may therefore result in cortical 'disconnection' which may significantly impair brain function, the so-called 'disconnection hypothesis' of age-related cognitive decline (8).

Damage to white matter can be assessed using several MRI modalities including structural, diffusion tensor (DT-) and magnetization transfer (MT-) MRI. DT-MRI measures the random macroscopic motion of water molecules in tissue, and is exquisitely sensitive to changes in white matter microstructural integrity (9). It provides two commonly used biomarkers, the mean diffusivity ($\langle D \rangle$) and fractional anisotropy (FA), the former indicating the magnitude and the latter the directional coherence of water molecule diffusion; parameters that can be measured either within regions of interest (ROI) or tracts segmented using tractography (10–12). $\langle D \rangle$ takes low and FA takes high values in healthy, structurally intact white matter, but rise or fall, respectively, in diseased tissue (8). DT-MRI studies report linear or even higher-order trends of increased $\langle D \rangle$ and decreased FA with advancing age (13), possibly with an anteroposterior gradient (12, 14, 15). These parameters correlate significantly with cognitive ability, in particular information processing, executive function and memory (16, 17), although with considerable individual variability (18). MT-MRI provides a further biomarker, the magnetization transfer ratio (MTR), which measures the efficiency of magnetization exchange between the relatively free water protons inside tissue and those bound to protein macromolecules in cellular membranes. In healthy, well-myelinated white matter MTR takes relatively high values (30–50%), but is reduced in pathological states, such as inflammation or demyelination (19), where compromised membrane integrity and absence of macromolecules leads to incomplete coupling between the two pools; MTR declines slowly with normal aging (20). DT- and MT-MRI therefore provide different, but complementary quantitative measures of white matter integrity that can be employed to investigate relationships between brain structural connectivity and cognitive aging.

Overt white matter damage is commonly observed in the form of white matter lesions (WMLs) that appear as regions of patchy hyperintense signal on T₂-weighted (T2W) and fluid attenuated inversion recovery (FLAIR) structural MRI in deep and periventricular white matter, basal ganglia and brainstem. These were once considered to be a silent consequence of aging and of no clinical relevance, but are now recognized to be associated with increased risk of future stroke, cognitive impairment and dementia (21–25). On DT- and MT-MRI, WMLs have higher $\langle D \rangle$, and lower FA and MTR than surrounding normal-appearing white matter (26); WML $\langle D \rangle$ is higher in subjects with more lesions, indicating more tissue damage when WMLs are more frequent (27); and $\langle D \rangle$ in normal-appearing white matter is also increased with higher WML scores indicating that normal-appearing tissue is more abnormal when the WML load is greater (27). Correlations between DT- and MT-MRI biomarkers in WMLs show that they are characterized by alterations in brain water homeostasis, reductions in white matter integrity and myelin injury (26). Measuring quantitative longitudinal relaxation time (T₁) values in WMLs, which is related to brain water content (28), in addition to signal intensity on structural MRI and DT- and MT-MRI biomarkers, may also be instructive in characterizing their pathophysiology.

Although of uncertain etiology, WMLs are associated with other features of cerebral small vessel disease including both clinically evident and silent small vessel (lacunar) stroke (29), lacunes (30), enlarged perivascular spaces (EPVS) (31) and brain microbleeds (32), which in turn are associated with old age cognitive decline (30, 32, 33). EPVS are a marker of blood-brain barrier disruption in lacunar stroke (34) and, in addition, inflammation in multiple sclerosis (35). Perivascular spaces are important conduits for drainage of interstitial fluid to the ventricular or cortical CSF and may represent an early stage in the development of WMLs. Mineral deposits, visible as hypointense areas on T₂*- (T2*W) or T₁-weighted (T1W) MRI, form in the basal ganglia where the perforating arterioles enter the brain and, although largely overlooked in previous studies, also indicate small vessel damage (36). These mineral deposits, which correspond with basal ganglia hyperattenuation on CT, have long been assumed to be calcium and largely ignored as physiological unless extreme, but include iron and possibly other minerals as well as calcium. Measuring DT- and MT-MRI biomarkers in those subjects with significant WMLs, EPVS, mineral deposits and microbleeds may provide insights into how these features affect normal-appearing white matter and their interrelationships.

These structural alterations observed mostly in cross-sectional imaging studies may, however, be related to events much earlier in life, and not all attributable just to advancing age (37). For example, the size and function of the brain in old age is likely related to its size and functional ability in early life, and even to *in utero* factors (38–40). Resistance to vascular disease and its effects on the heart, brain and other organs may also be 'preset' *in utero* (40). Genetic, and early life social, environmental, educational and nutritional factors may, therefore, all interact

and lead to events in adulthood that influence the state of the brain and its vulnerability to additional insults in old age (41–46).

Several large imaging studies have investigated changes in brain structure and cognitive function, either with cross-sectional and serial assessments, e.g. the Rotterdam Scan Study (22, 47), the Cardiovascular Health Study (48), LADIS (27, 49), or just one cross-sectional assessment, e.g. the SMART-MR study (50) and RUN DMC (51). While these studies have identified imaging features that are associated with impaired cognition, none have been able to correct for early life cognitive ability. This is important as cognitive ability measured in old age is a function of premorbid ability and how much it has changed over adult life. Most have included subjects with a range of ages so that relationships between imaging features and cognition may have been confounded by rapid changes in certain parameters, such as $\langle D \rangle$ and FA (13), even after correcting for age, and by parallel aging trends.

In this paper, we describe the brain MRI and neurovascular ultrasound imaging protocol developed to study the Lothian Birth Cohort 1936 (LBC1936), a group of subjects in whom cognitive data are available in both youth and old age. Members of this cohort were born in 1936 and took a well-validated test of intelligence, a version of the Moray House Test No. 12, in the Scottish Mental Survey of 1947 (52). The test results were retained by the Scottish Council for Research in Education, who administered the Survey. People born in 1936 and living in the Edinburgh area were contacted and invited to participate in a wide-ranging study to find determinants of nonpathological cognitive aging (53). Between 2004 and 2007 (Wave 1), 1091 people, then aged around 70 years, retook the Moray House Test and other detailed cognitive and physiological tests, and provided social, family, nutritional and medical histories, samples for blood biomarkers and genetic analysis, quality of life and physical activity information (53). Now approximately 3 years older, the LBC1936 subjects have been invited to participate in a second wave of testing, which now additionally includes brain MRI and neurovascular ultrasound imaging (Wave 2). A third wave of cognitive, physiological and social assessments, and a second wave of MRI are planned for 2011–2013 (Wave 3). In all three waves, the specific cognitive domains tested include executive function, immediate and delayed verbal declarative memory, verbal learning and memory, non-verbal spatial learning and memory, constructional ability, prior cognitive ability, working memory and speed, and variability of simple information processing (53). The average age of this large cohort is ideal for studying normal aging because brain structure and cognitive ability change rapidly after 70. Moreover, the narrow age range, they are all born in the same year, is critical in obviating the problem where chronological age heavily confounds the influence of other variables, such as the significant dependence of $\langle D \rangle$ and FA on age (13). The imaging data, in addition to genetic and lifestyle information, and the availability of life-long measures of cognitive ability, provide an unparalleled opportunity to study relationships between brain structure and cognitive aging.

We shall test two primary hypotheses. Firstly that age-related cognitive decline, especially the fundamental efficiency of information processing, is affected by cortical disconnection through declining white matter integrity after correcting for early life cognitive ability; and secondly that vascular and genetic risk factors, diet, education, physical exercise and other life course events influence the age of onset, the severity and occurrence of white matter damage and this is related to individual differences in cognitive decline. We also plan to test several individual hypotheses related to specific imaging features, namely that (i) decreasing integrity in normal-appearing white matter will be associated with an increase in WML load, EPVS, mineral deposits and microbleeds; (ii) typical age-related features of brain damage, brain atrophy, declining white matter integrity and WMLs, will occur in different proportions in different subjects and will be associated with impairments in different cognitive domains, and with different vascular, genetic and other risk factors; and (iii) imaging biomarkers derived from DT-, MT- and T_1 -mapping protocols will provide insights into the pathophysiology of WMLs and be linked to severity and signal intensity values on structural MRI that can be tracked in longitudinal studies.

Methods

Subjects and study design

The LBC1936 comprises 1091 community-dwelling healthy individuals without dementia. Subjects were identified when aged about 70 and had detailed cognitive and other nonimaging assessments; full details of the recruitment and testing have been described in detail previously (53). The study is an observational, longitudinal cohort study with blinded outcome assessments and analyses.

Brain MRI acquisition protocol

All MRI data are acquired in the Brain Research Imaging Centre, University of Edinburgh (<http://www.bric.ed.ac.uk>), using a GE Signa Horizon HDx 1.5 T clinical scanner (General Electric, Milwaukee, WI) equipped with a self-shielding gradient set (33 mT/m maximum gradient strength) and manufacturer supplied eight-channel phased-array head coil. The examination comprises the following whole-brain sequences acquired with contiguous slice locations: T2W, T2*W and FLAIR axial scans, a high-resolution T1W volume sequence acquired in the coronal plane, axial T1W fast-spoiled gradient echo (FSPGR) sequences with 2° and 12° flip angles for quantitative T_1 -mapping, two standard spin echo sequences acquired with and without a MT pulse applied 1 kHz from the water resonance frequency for MT-MRI, and finally a DT-MRI protocol consisting of seven T2W and sets of diffusion-weighted ($b = 1000 \text{ s/mm}^2$) axial single-shot spin-echo echo-planar (EP) volumes acquired with diffusion gradients applied in 64 noncollinear directions (54). The acquisition

takes approximately 70 min (see Fig. 1 and Table 1 for images and sequence details). The acquisition parameters for the T2W, T2*W, FLAIR, DT-, MT- and T₁-mapping protocols, i.e. field-of-view, imaging matrix, slice thickness and location, have been chosen to allow easier coregistration between sequences so that $\langle D \rangle$, FA, MTR and T₁ biomarkers can be accurately measured in features such as WMLs identified on the structural scans. To allow accurate measurement of intracranial volume (ICV), the structural MRI scans cover the complete intracranial contents, from above the skull vertex to the upper cervical spine below the foramen magnum. All structural MRI data are examined by a consultant neuroradiologist and any medically relevant incidental findings, which occur in around 3% of individuals and not including age-related WMLs (55), are identified and notified to a responsible clinician for further action. Finally, each sequence is converted from DICOM (<http://dicom.nema.org>) to either ANALYZE 7.5 (<http://www.analyze-direct.com>) or NIFTI-1 (<http://nifti.nih.gov/nifti-1>) format for computational image processing.

Carotid and vertebral ultrasound acquisition protocol

Neck artery ultrasound imaging is performed on a Siemens Antares Premium Colour Doppler scanner (Siemens AG, Erlangen, Germany) with 7.5 MHz variable frequency probe by one of the three experienced neurovascular ultrasonogra-

phers. Representative velocity readings are obtained of the common, internal and external carotid and vertebral arteries (56). The presence and location of atheromatous stenosis, including whether it appears smooth or irregular (ulcerated) (57), is documented. Percent stenosis is quantified based on velocity criteria, while measurements of lumen reduction are expressed in North American Symptomatic Carotid Endarterectomy Trial format (58). Common carotid and carotid bulb intima-media thickness (IMT) is measured manually with callipers and using the Framingham Heart Study IMT software available on the ultrasound scanner. This measures minimum, maximum and mean IMT over a 1 cm long segment of the common carotid artery and carotid bulb using the average of three measurements (59, 60). IMT is an indirect measure of vascular risk and is associated with large artery atherosclerosis rather than small vessel disease (61, 62). As such it is a useful marker of the impact of vascular risk factors on individual subjects and their ability to withstand the insult.

Assessment of imaging features and structural MRI analysis

A reliable, fully automatic method for quantifying all features of aging on MRI, whether focal or diffuse, normal anatomical structures or otherwise, does not yet exist. We, therefore, use a combined approach of qualitative visual rating scales performed by expert neuroradiologists and computational image processing

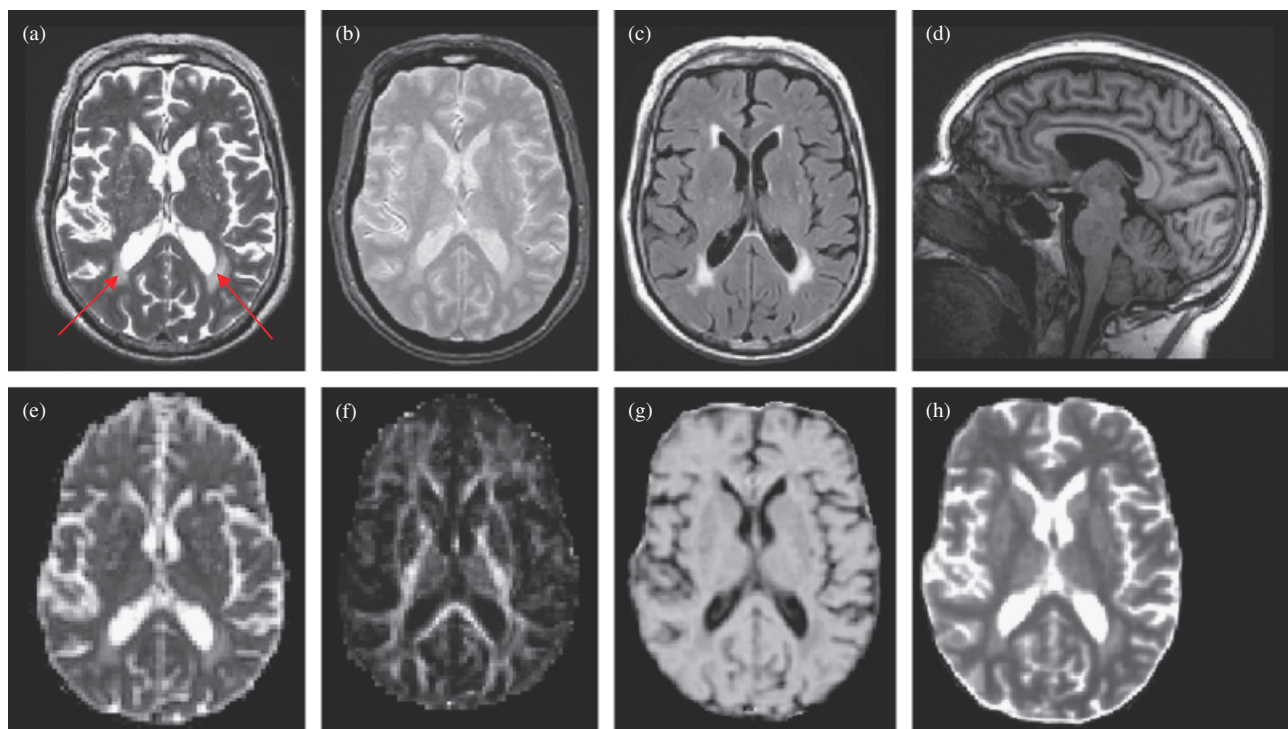


Fig. 1 An example of the different scan data acquired in the brain MRI protocol (see Table 1); (a) T₂-weighted, (b) T₂*-weighted, (c) FLAIR-weighted, (d) high-resolution T₁-weighted volume, (e) mean diffusivity ($\langle D \rangle$), (f) fractional anisotropy (FA), (g) magnetization transfer ratio (MTR) and (h) quantitative T₁ relaxation time maps from a representative subject. All maps are obtained from the same slice location except (d). White matter lesions are indicated by the red arrows in (a). Note the increased $\langle D \rangle$ and T₁, and reduced FA and MTR of these lesions compared with surrounding normal-appearing white matter.

Table 1 Sequence parameters for MRI scanning

| Sequence name | Acquisition method | Field-of-view (mm) | Matrix | Slices | Thickness (mm) | Voxel (mm) | TR/TE/TI (ms) |
|---------------------------------------|--------------------|--------------------|------------|--------|----------------|-------------|---------------|
| T ₂ -weighted | FSE | 256 × 256 | 256 × 256 | 80 | 2 | 1 × 1 × 2 | 1 1320/105 |
| T ₂ [*] -weighted | Gradient echo | 256 × 256 | 256 × 192* | 80 | 2 | 1 × 1 × 2 | 940/15 |
| FLAIR | FSE | 256 × 256 | 256 × 192* | 40 | 4 | 1 × 1 × 4 | 9002/147/2200 |
| T ₁ -weighted volume | 3D IR-Prep FSPGR | 256 × 256 | 192 × 192* | 160 | 1.3 | 1 × 1 × 1.3 | 10/4/500 |
| Diffusion tensor | Single-shot SE EPI | 256 × 256 | 128 × 128 | 72 | 2 | 2 × 2 × 2 | 16 500/98 |
| Magnetization transfer | SE | 256 × 256 | 128 × 128* | 72 | 2 | 1 × 1 × 2 | 3520/10 |
| T ₁ -mapping | FSPGR | 256 × 256 | 128 × 128* | 72 | 2 | 1 × 1 × 2 | 6/2 |

*Zero filled to 256 × 256. SE, spin echo; FSE, fast spin echo; IR-Prep, inversion recovery prepared; FSPGR, fast spoiled gradient echo; EPI, echo planar imaging.

methods, both performed blind to all subject and imaging data. In some cases, where a similar metric is measured, e.g. WML score and volume, then the qualitative and quantitative methods are complementary and act as validation tools.

For the qualitative visual rating we record the presence and amount of cortical and subcortical infarcts, old primary hemorrhages, cortical siderosis, microbleeds, deep and periventricular WMLs, WMLs in specific white matter pathways, EPVS, microbleeds, mineral deposits in the basal ganglia and superficial and deep brain tissue loss (see Table 2 for definitions). Most of these features are either markers of small vessel damage, e.g. WMLs, EPVS and microbleeds, large artery stroke, or of several different processes, e.g. atrophy. There are numerous scales for quantifying WMLs. Some have floor or ceiling effects so are of limited use in some populations, while others do not distinguish deep from periventricular WMLs, and yet others are very detailed without there being a clear benefit from the added time required to apply them. We previously tested several scales in the same dataset (63) and found that the Fazekas scale (64) performed extremely well, without floor or ceiling effects, and was quick to apply. It is also one of the oldest and most widely used scales and therefore the results are generalizable to other studies and populations. We also use two other scales that focus on more specific lesion distributions. One of these, the Wahlund scale (65), rates WMLs in more detailed brain subregions, i.e. major lobes, basal ganglia and brainstem/cerebellum, is quick to apply, and provides an anatomical substrate against which the cognitive data can be compared. The other is the Bocti scale (66) developed to quantify lesions in the cholinergic pathways that are thought to be involved in memory. Because memory decline is common in aging, we felt it was particularly important to look for overt evidence of WMLs specifically affecting these pathways. Hence, WMLs are scored on the FLAIR and T2W volumes using the Fazekas (coding separately for deep and periventricular lesions), Wahlund and Bocti scales. For each scale, the left and right hemispheres are scored separately and combined to give an overall value indicating the highest WML score. The number of EPVS in the hippocampus, basal ganglia and centrum semiovale are coded in the left and right hemispheres separately, and overall, using a validated scale developed 'in house' which is similar to other rating scales (33, 67). Infarcts are coded for size

and location based on vascular territory using a validated stroke lesion rating scale (68), which differentiates infarcts into cortical, lacunar, border zone and brainstem/cerebellar. Old hemorrhages are also coded by size and location (68). Lacunar infarcts are coded as having cavitated or not, because although only about 20% of symptomatic lacunar infarcts cavitate (69), such lesions likely indicate a greater degree of tissue damage which could be associated with worse cognitive function. Microhemorrhages are coded for number and distribution using a simplified version of the Brain Observer MicroBleed Scale (70), which we developed in a similar population to the LBC1936. Hemosiderin and other mineral deposits are rated using a general scale that includes all microbleeds, basal ganglia mineral deposits and prior hemorrhages (37, 71). As a guide to estimate the volume of iron deposits in the brain, one 5 mm diameter microbleed has, on average, a volume of 8 mm³. Finally, brain atrophy is coded using a validated template developed from T1W and T2W data acquired from normal subjects aged 65–70 years (7), with superficial and deep atrophy coded separately according to the centile of the population of 65–70-year-olds that they most closely match.

Quantitative structural image analysis includes measurement of volumes of the intracranial compartment, total CSF, whole brain, ventricles, gray matter, normal-appearing white matter, WMLs and their spatial distribution, brain subregions (hippocampus, major lobes), and brain mineral (basal ganglia, microbleeds, siderosis) deposits. For tissue segmentation, we developed a semiautomatic segmentation tool in which two MRI sequences are fused in red–green color space to enhance visual differences between tissues and allow specific features of interest to be extracted (74). This method, named 'MCMxxxVI' (standing for 'Multispectral Colouring Modulation and Variance Identification', and also being the Roman numerals for 1936 as in LBC1936), employs Minimum Variance Quantization, as implemented in the MATLAB (<http://www.mathworks.com>) function 'rgb2ind', to represent images in a reduced number of clusters mapped in the same color space. This algorithm uses the Floyd–Steinberg's error diffusion dither principle in which more color map entries are allocated to densely populated areas in the color space and fewer entries to infrequent colors thereby delivering enhanced clusterization (75). In practice, the T1W, T2*W and FLAIR

Table 2 Definitions of key imaging features of aging on structural MRI

| Structure | Definition |
|--------------------------------------|---|
| White matter lesions | Diffuse, patchy areas distributed either in the deep or periventricular white matter, basal ganglia or brain stem. They are > 3 mm in diameter and are hyperintense with respect to normal-appearing gray and white matter on T2W and FLAIR, but not as hyperintense as CSF on T2W. They may be slightly hypointense on T1W but not as hypointense as CSF (64). For computational image analysis, the definition of Payne was used to avoid accidental inclusion of artifacts (72). |
| Enlarged perivascular spaces | Small punctate or linear hyperintensities, in axial and longitudinal section respectively, on T2W that are < 3 mm in diameter in white matter or basal ganglia. Larger ones may be visible on T1W as decreased signal but not visible on T2*W or FLAIR (31). |
| Infarcts | Defined as per standard textbook definitions in cortex, small or large subcortical or border zone (67). Lacunes, or cavitated lacunar lesions, defined as small, > 3 mm and < 2 cm in diameter, subcortical lesions of increased signal on T2W and decreased signal on T1W and FLAIR. |
| Old hemorrhages | Identified by the presence of low signal due to hemosiderin on T2*W. |
| Microbleeds | Small, < 5 mm diameter, homogeneous, round foci of low signal intensity on T2*W in white matter, basal ganglia or at the cortico-subcortical junction that are not simply flow voids in small vessels (32, 70). |
| Mineral deposits | Mainly composed of iron oxyhydroxide that accumulates in insoluble form in brain tissue, typically in the basal ganglia and identifiable as very hypointense regions on T2*W (71). Presence of calcium and other minerals is indicated if the signal is hypointense on both T2*W and T1W (73). |
| Brain atrophy | Loss of gray and white matter with enlargement of the CSF containing spaces. Can mainly affect deep structures resulting in ventricular enlargement or cortex resulting in sulcal enlargement, or both. |
| Intracranial volume | All structures inside the dura; lower limit defined as the axial slice immediately inferior to the inferior limit of the cerebellar tonsils and on or above the superior tip of the odontoid process. |
| Brain volume | ICV minus CSF volume. |
| Ventricular volume | Volume of lateral, third and fourth ventricles and aqueduct. |
| WML volume | Measured in the cerebral hemispheres, cerebellum and brainstem, and quantified semi-automatically with MCMxxxVI (74) by fusing T2*W and FLAIR volumes. False-positive lesion in the insular cortex, cingulate gyrus, anterior temporal cortex and around the floor of the third ventricle are removed manually. |
| Normal-appearing white matter volume | Automatically segmented by fusing the T1W and T2W sequences (see Fig. 2). |
| Gray matter volume | Deep and cortical gray matter extracted by subtracting CSF, white matter and WML masks from the ICV mask. |
| Hippocampal volume | Measured using FSL FIRST on the T1W volume scans using an age-appropriate registration template (7), followed by manual editing. This method has been validated against the 'gold-standard' approach of manual tracing. |
| Mineral deposit volume | Hemosiderin deposits are semi-automatically segmented by fusing T2*W and FLAIR volumes in which they appear green in the fused color space (see Fig. 3). A manual postprocessing step is used to remove false positives, e.g. major arteries and venous sinuses. |

scans are registered to the T2W sequence using FLIRT (76), an affine registration tool from the FMRIB software library (FSL; <http://www.fmrib.ox.ac.uk/fsl>), with different pairs of volumes combined to identify different brain structures (see Figs. 2 and 3). Fusion of T1W and T2W volumes is best for identifying CSF and normal-appearing white matter, while T2*W and FLAIR is best for identifying WMLs. The resulting tissue masks are stored in ANALYZE or NIFTI-1 format, with the volume for each structure given in mm³. A semiautomatic method to identify and count EPVS is currently being developed.

We measure ICV as it provides an estimate of maximum adult brain size in youth and is required to determine brain atrophy and to normalize other volumes. A whole-brain mask is initially obtained from the T2*W volume with the Object Extractor Tool from ANALYZE 10.0 and then edited to remove erroneous tissue by applying it to a fused T1W/T2W or T2*W/FLAIR volume pair produced with MCMxxxVI.

Finally, hippocampal volume is measured using a semiautomated, atlas-based segmentation approach based on FSL

FIRST, normalized to an age-appropriate normal template (7). The results are visually inspected and, where necessary, corrected by manual editing which is needed in approximately 2/3 of cases. We have tested the accuracy of this approach against manually measured hippocampal volume with detailed visual comparison in 120 subjects and found the automated segmentation to be too inaccurate without manual editing. However, the automated step reduces the amount of time taken to measure hippocampal volume considerably.

DT, tractography, MT and T₁-mapping analysis

The microstructural integrity of white matter for whole brain, different regions and in a range of major tracts is measured using histogram, ROI and tractography analysis of the DT-, MT- and T₁-mapping MRI data. The DT-MRI data are preprocessed using FSL tools to extract the brain (77) and remove bulk patient motion and eddy current induced artifacts by registering the diffusion-weighted to the first T2W

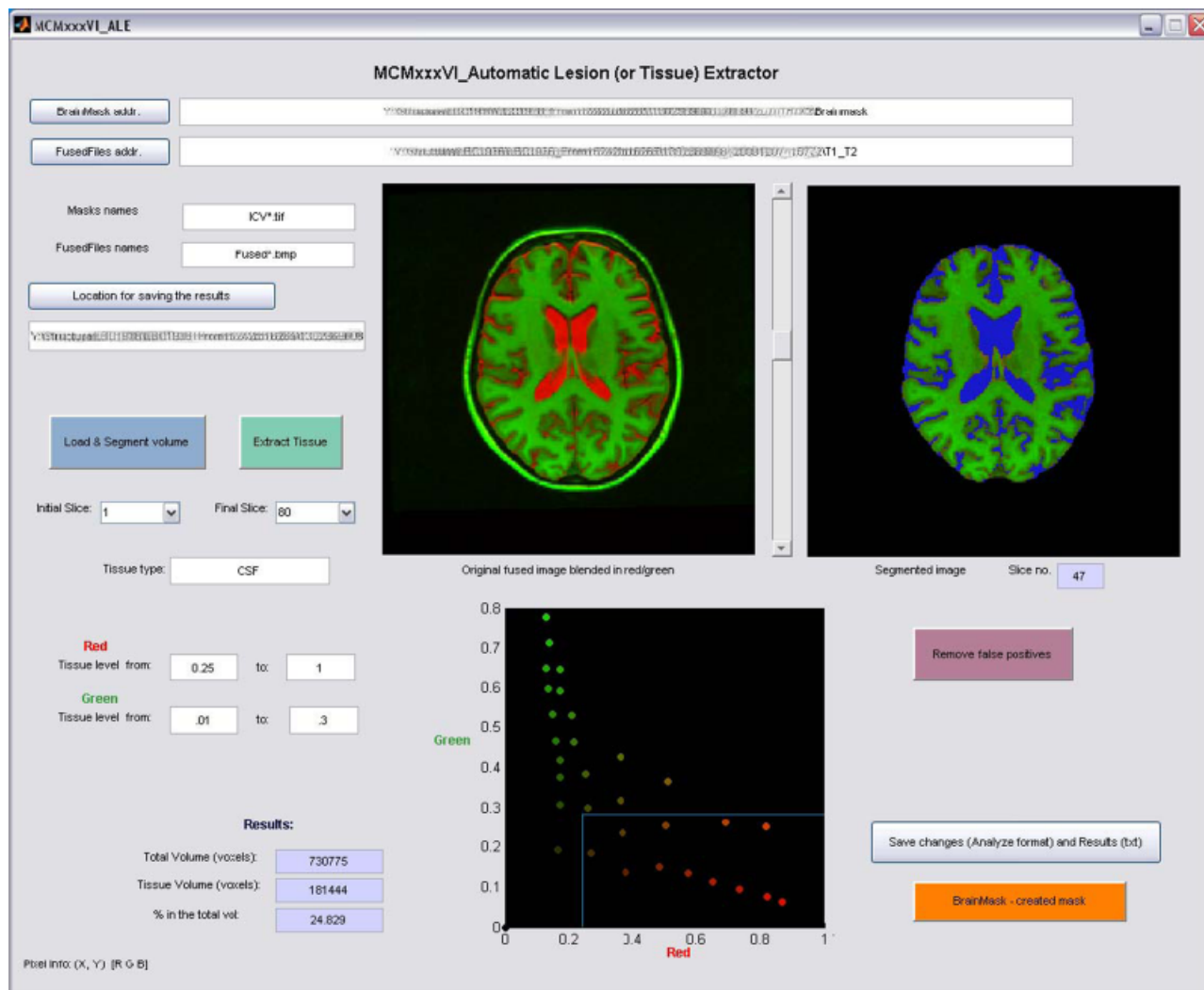


Fig. 2 Screen capture of the segmentation module of the MCMxxxVI tool illustrating CSF extraction in a slice of registered and fused T1W and T2W volumes. In this example, CSF is represented in red (left-hand image) and blue (right-hand image) before and after brain extraction, while the bright green colors indicate normal-appearing white matter. The clusters that correspond to each tissue type are represented in a graph in the normalized red–green (RG) color space. Moving the cursor over the brain produces values of the RG coordinates of the corresponding cluster. These values are then inputted as the maximum and minimum thresholds in each color, with the software tool automatically constructing a mask of the tissue of interest.

($b = 0 \text{ s/mm}^2$) EP volume for each subject (76). $\langle D \rangle$ and FA volumes are created using DTIFIT. The underlying connectivity data are generated with BedpostX and ProbTrackX ran with its default parameters of a two-fiber model per voxel, 5000 probabilistic streamlines for each tract with a fixed separation distance of 0.5 mm between successive points (78).

Quantitative maps of T_1 are obtained by registering the 2° and 12° FSPGR sequences to the T2W volume scan using FLIRT, with T_1 being determined from

$$\frac{1}{T_1} = \frac{1}{T_R} \ln \left[\frac{S_R \sin \alpha_2 \cos \alpha_1 - \sin \alpha_1 \cos \alpha_2}{S_R \sin \alpha_2 - \sin \alpha_1} \right], \quad (1)$$

where T_R is the repetition time ($= 6 \text{ ms}$), $\alpha_1 = 2^\circ$, $\alpha_2 = 12^\circ$, $S_R = S_1/S_2$, and S_1 and S_2 the signal intensity values in each voxel for α_1 and α_2 respectively (79). Similarly maps of MTR

are obtained by registering the two-component spin echo sequences to the T2W volume and calculated this biomarker on a voxel-by-voxel basis using

$$\text{MTR} = 100 \frac{M_0 - M_s}{M_0}, \quad (2)$$

where M_s and M_0 represent signal intensities with and without the MT pulse (20, 26). Examples of $\langle D \rangle$, FA, T_1 and MTR maps for a representative subject are shown in Fig. 1.

We used probabilistic neighborhood tractography (PNT), as implemented in the TractoR package for fiber tracking and analysis (<https://github.com/jonclayden/tractor>), to segment the same fasciculus in each subject from BedpostX/ProbTrackX single-seed point tractography output using probabilistic tract shape modelling (80–82). In PNT, seed points are

automatically placed in a neighborhood (typically $7 \times 7 \times 7$ voxels) surrounding a seed point transferred from standard space, with the tract that best matches a predefined reference tract in terms of both length and shape chosen from this group of 'candidate' tracts (see Fig. 4). This ability to quantify how the length and shape of a specific tract differs from that of a reference for each subject is unique to PNT, and allows a detailed investigation into how tract topology, in addition to tract-averaged water diffusion parameters, changes within a population (82). This topological information is provided by the likelihood log-ratio, R , which indicates the goodness-of-fit in terms of length and shape between the reference and the best match tract (80–82). Tract-averaged water diffusion parameters are determined by applying the best match tract mask to each subject's $\langle D \rangle$ and FA volumes. This method has test-retest coefficients of variation for tract-averaged FA across several tracts of 4–8%, which compares favorably with other studies using tractography to segment tracts (81). Owing to significant computational requirements, this analysis is performed on a high-performance cluster (1456 cores), running an industry standard Linux-based operating system (<http://www.ecdf.ed.ac.uk>).

Affine registration of DT-, MT- and T_1 -mapping MRI data supply whole brain (histogram), regional (ROI in normal-appearing white matter and WMLs) and tract-specific (tractography) measurements of $\langle D \rangle$, FA, MTR and T_1 . Tracts segmented using PNT include genu and splenium of corpus callosum, rostral and ventral cinguli, arcuate, uncinate and inferior longitudinal fasciculi and anterior thalamic radiations (see Fig. 4b). For each segmented tract, the topological similarity (or difference) to the predefined reference tract is given by R .

Sample size estimation

We have calculated the power of the study based upon an N of 650, which will be the minimum number of subjects providing data for each of the above imaging variables. We set α at 0.05 (two-tailed), and power at 80%, and calculated the effect size the study will be able to detect using nQuery Advisor (<http://www.statistical-solutions-software.com>). For bivariate correlation using Pearson's method, the study has 80% power to detect an r -value of 0.11. For multiple linear regression, in a model in which an imaging biomarker is being added when

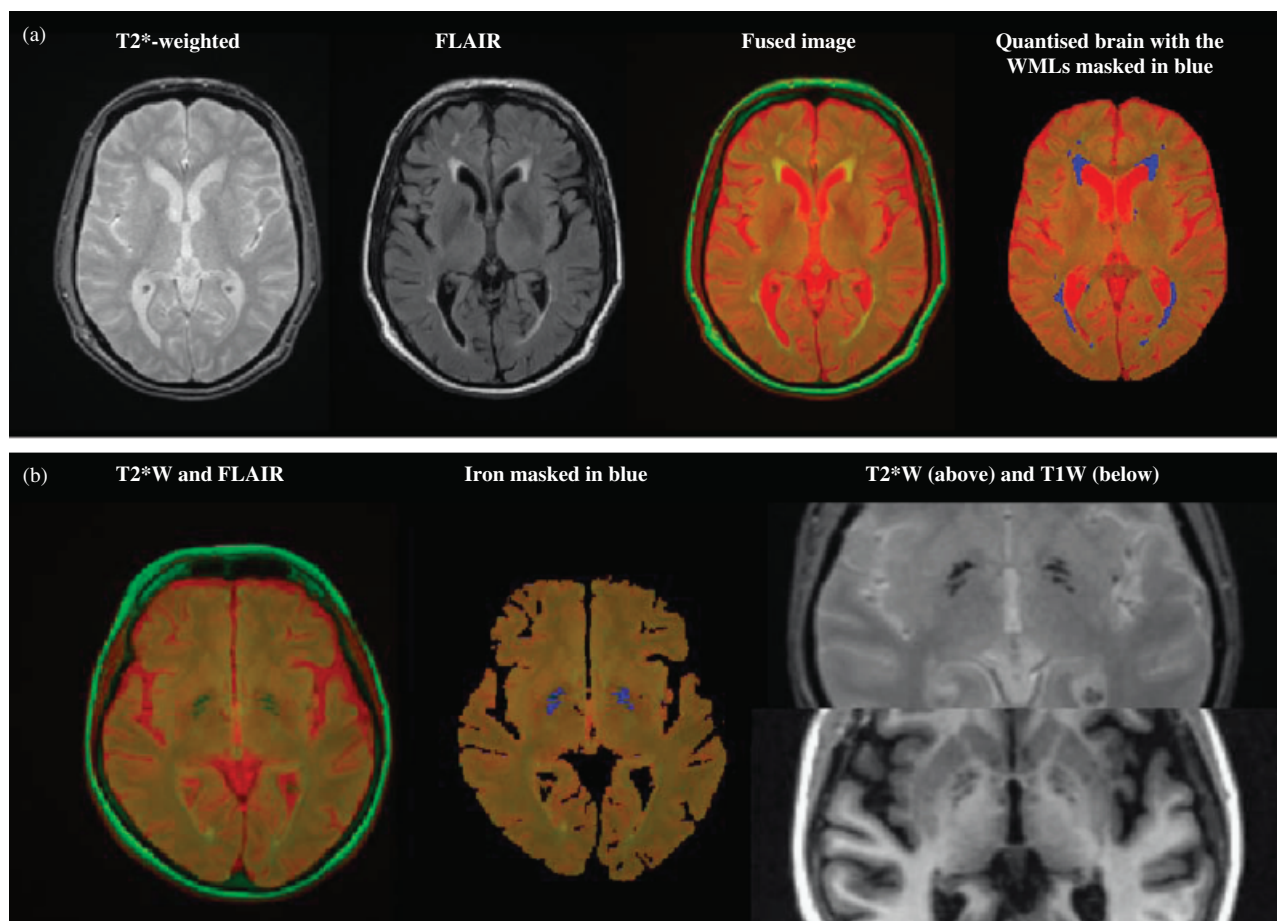


Fig. 3 Example of brain regional volumes measured using MCMxxxVI, in this case WMLs (a), and iron and calcium deposits (b). In (b), all regions that contain iron or calcium deposits are hypointense on T2*W; however, regions that contain calcium deposits appear hypointense on T1W, while regions with only iron produce no signal change (taken from (37)).

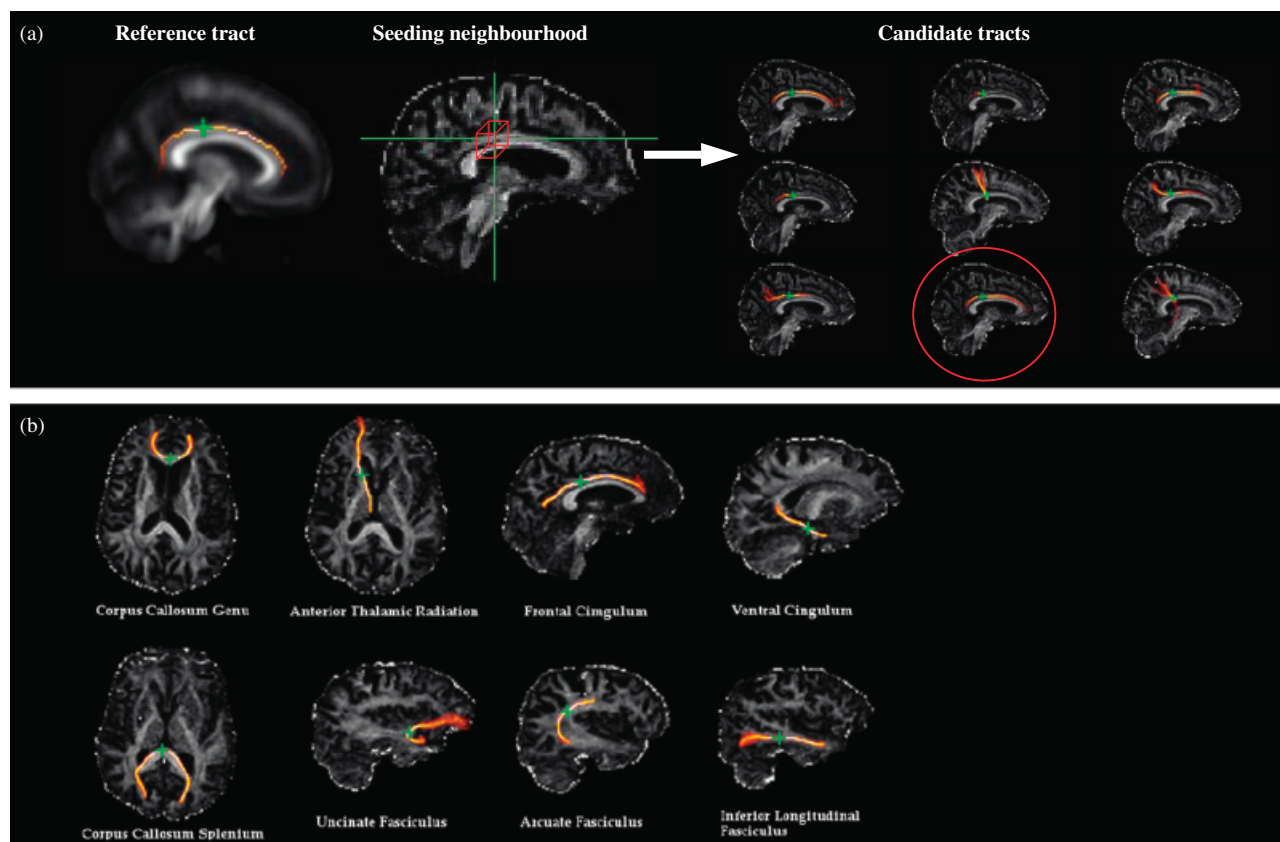


Fig. 4 (a) Schematic diagram showing the PNT processing pipeline. Given a predefined reference tract, in this case rostral cingulum, seed points are automatically placed in a neighborhood surrounding a seed point transferred from standard space (red box). The tract that best matches the reference in terms of both length and shape (red circle) is chosen from this group of 'candidate' tracts. (b) Examples of the tracts segmented in this study for a representative subject.

four prior covariates have already accounted for 40% of the variance in the outcome, the study has 80% power to detect a variable contributing another 0.72% of the variance. In both of these examples, the study, therefore, has good power to detect even small effect sizes, and it is arguable that any clinically relevant effects will be considerably larger than this, and the study will have correspondingly greater power to detect such effects. Where considerably more power is required, such as in genome-wide association studies, we have joined consortia, e.g. Enigma (<http://enigma.ion.ucla.edu>), to allow meta-analysis of results.

Statistical analyses

We shall investigate associations between normal and abnormal structural features, $\langle D \rangle$, FA, MTR and T_1 values measured in ROIs placed in standardized brain regions in normal-appearing white matter, in WMLs and in a range of major white matter tracts, and cognitive ability measured in both youth and old age. Associations will be examined using correlation and general linear modelling, e.g. via regression and ANCOVA methods. To understand the data more fully requires structural equation modelling (SEM), which can explicitly explore mediation effects, latent traits and multiple

outcome variables. A general factor of cognitive ability (g), memory (g_{memory}) and information processing speed (g_{speed}) will be obtained using principal component analysis from the cognitive data (83). In previous studies of white matter and cognition, SEM has shown that the influence of hypertension on cognition is mediated via WMLs (23), and that the association between FA and cognition is mediated via speed of information processing (16). Similar approaches will be applied to the imaging data to assess relationships between brain structure and cognitive ability. For example, in preliminary analyses of eight white matter tracts in 132 LBC1936 participants, we have shown that white matter tract integrity, represented by a general factor (high values indicate structurally intact fibers), has a significant negative correlation with g_{speed} (higher values indicate slower information processing speed) (83). Correcting any associations between old age cognition and imaging biomarkers with cognitive ability measured at age 11 years is essential to determine how cognitive ability in later life is affected by age-related change and early life status. For example, in a preliminary analysis of brain mineralization and cognition, we found that although increased mineral deposits at age 72 years were associated with poorer performance on cognitive tests taken at the same age, most of this association disappeared when the analysis was

corrected for age 11 cognitive ability (37). Identifying mechanisms of reverse causation are important in order to avoid the assumption that all cognition–structure associations in older age are the consequence of aging, and embarking on intervention trials of treatments, e.g. drinking large amounts of coffee (84), that may be ill founded.

Study organization and funding

The study is funded from several sources, namely Age UK for the Disconnected Mind Project (<http://www.disconnected-mind.ed.ac.uk>), as a major gift campaign, and the Sydney De Haan Award (Ref no. 285); the UK Medical Research Council (MRC) project ‘Brain white matter imaging and cognitive aging in the Lothian Birth Cohort of 1936’ (Ref no. 82800), which funds the imaging staff; BBSRC (Ref no. BB/F019394/1) for genetic aspects; the MRC Centre for Cognitive Ageing and Cognitive Epidemiology (CCACE, funding for I. J. D.); the Chief Scientist Office through NHS Lothian Research and Development (part-funding for Z. M.); the Scottish Funding Council (SFC) through the Scottish Imaging Network, a Platform for Scientific Excellence (SINAPSE, <http://www.sinapse.ac.uk>) Collaboration (part-funding for J. M. W. and E. M. S.); the Scottish Academic Health Sciences Collaboration through NHS Lothian (part funding for E. M. S.). The study is approved by the Lothian (REC 07/MRE00/58) and Scottish Multicentre (MREC/01/0/56) Research Ethics Committees and all subjects give written informed consent. The brain imaging study is a collaboration between the Departments of Clinical Neurosciences, Medical Physics, Psychology, Geriatrics and the Brain Research Imaging Centre, University of Edinburgh. Blood samples, cognitive testing and other related physiological assessments are performed in the Edinburgh Wellcome Trust Clinical Research Facility (WTCRF, <http://www.wtcrf.ed.ac.uk>) by trained psychologists and nurses. All MRI and image analysis are performed in the Brain Research Imaging Centre, where the MRI scanner is monitored with a quality assurance program to maintain image quality at an optimum level. The study data are held in a database in the Department of Psychology, double entered and cross checked for accuracy. Steering (I. J. D., J. M. W., M. E. B., J. M. S.) and image analysis (J. M. W., M. E. B., M. C. V. H., S. M. M., N. A. R.) committees meet monthly to review overall study and data analysis progress.

Summary

We have described the brain MRI and vascular ultrasound imaging of a unique group of subjects, the LBC1936, in whom cognitive data are available in both youth and old age. To utilize the full potential of this cohort for studying how early life intelligence, and brain structure, genetic and vascular risk factors in later life affect cognitive aging, we have developed state-of-the-art imaging and analysis protocols to identify and quantify brain atrophy, WMLs and their spatial distribution,

brain mineralization, integrity and topology of major white matter tracts and the health of neck arteries. For example, we have developed a segmentation tool for measuring WMLs that avoids the systematic bias found in FLAIR thresholding methods, and adapted it to identify brain mineral deposits and measure different brain regional volumes (37, 74). We have also devised a novel tractography method that is able to quantify changes in tract shape resulting from global and region atrophy (82). In addition to quantitative approaches, we also use qualitative visual rating scales to score WMLs, EPVS, infarcts, microbleeds, mineral deposits and brain atrophy as these scales automatically account for relative brain size, whereas quantitative measurements have to be normalized by some factor, such as ICV, which can distort associations between some features (38). As well as complementing the computational image processing, the visual qualitative assessment has the added benefit of making the results directly translatable into current clinical practise, while the radiological reporting of scans is part of good research practice. In pilot analyses, this methodology has already shown that white matter integrity is substantially shared among tracts and the shared variance is associated with processing speed (83); and that the ancestral allele of one single-nucleotide polymorphism of the β_2 -adrenergic receptor gene is associated with splenium corpus callosum integrity and preserved cognitive ability (85).

The combination of structural, DT-, MT- and T_1 -mapping MRI protocols is a key strength of the study, and allows changes in normal- and abnormal-appearing gray and white matter to be measured simultaneously and linked to cognitive, genetic and vascular risk factors and mapped in longitudinal studies. This holistic approach is important because focusing on one feature, for example cortical tissue loss or WML load, may risk missing important coassociations or interactions that could provide a more complete picture of how and why the brain changes with age and relationships with vascular disease, cognition and physical health. For example, WMLs vary in number, distribution and signal intensity, i.e. ‘whiteness’ on T2W and FLAIR MRI, so simply measuring their volume will not distinguish between subjects with moderate numbers of lesions that are not particularly intense and subjects with moderate numbers of lesions that are very intense, even though the latter could indicate more severe white matter damage (86). Insights into how WML signal intensity relates to severity, the effects of WML location and prevalence on surrounding normal-appearing white matter, and aspects of their pathophysiology can be obtained through regional and tract-specific measurements of water diffusion, MTR and T_1 biomarker values (see Fig. 1). Finally, accurate quantification of regional brain volumes will allow associations between WML load and gray and white matter atrophy to be determined, which is important as WMLs and atrophy may develop at different rates and their interrelationships are, as yet, not well documented (87). For example, WMLs are associated with hippocampal atrophy in patients with Alzheimer’s disease, but whether this

is because Alzheimer's, WMLs and hippocampal atrophy are all common or because of specific interrelationships remains unclear (88). A potential weakness of the protocol is that we are unable to include several other imaging sequences that are of interest in the study of aging and/or cognition, such as resting state fMRI for brain connectivity, fMRI for specific cognitive tasks and transcranial Doppler ultrasound measurement of intracranial blood flow velocity. However, a longer acquisition would risk not just increasing noncompliance in the first wave of imaging, but would put subjects off coming back for repeat scanning, thus reducing the power and generalizability of the study.

It is frequently assumed that features seen on brain MRI of aging subjects are a consequence of being old, albeit tempered by the effects of life-long exposure to risk factors or adverse events. However, there is increasing evidence that many features in the brain in older age, including features detected by DT-MRI in normal-appearing white matter and overt lesions, may in fact be associated with early life factors (16). Specifically, in two pilot studies of the LBC1936 we found that having more iron deposits at age 72 years was significantly associated with lower general cognitive ability in youth and old age, and that the relationships with old-age general cognitive ability remained significant after controlling for childhood cognition (37); and that WML volume is not just associated with lower ability in all cognitive domains in old age, but that it is also associated with age 11 IQ (86). These results reinforce associations that were suggested in a smaller study of subjects scanned in their 80s, the LBC1921 (16), and clearly demonstrate the importance of having access to early life measures of cognitive ability in order to test for possible confounding or reverse causation in any contemporaneous association between cognitive ability and brain MRI biomarkers measured in old age. Therefore, this study is unusual in being able to differentiate effects that have early life influences from those that genuinely arise in old age, a vital step in developing strategies for successful cognitive aging.

Finally, insights into the sequence of events that lead to brain structural changes in old age and how they relate to cognitive decline will require longitudinal study. To achieve this goal, there will be a second wave of brain MRI and associated cognitive/physiological assessments in 2011–2013 (Wave 3). Repeat MRI will permit the determination, among other features, of brain atrophy rates across this population, changes in tract integrity and shape, brain mineralization, and increases in overt white matter damage. Even with the attrition rate expected in subjects of this age, the sample size will still be large enough to have sufficient statistical power to identify multiple overlapping risk factors and distinguish coassociated variables from potentially causative associations.

Acknowledgements

We thank the following: (i) the participants of LBC1936; (ii) Alan Gow, Caroline Brett, Caroline Cameron, Janie Corley,

Ross Henderson, Alison Pattie and Michelle Taylor for data collection and data entry; (iii) study data manager Paul Redmond and the study secretary Paula Davies; (iv) senior vascular ultrasonographer Avril Thomas, senior MRI radiographers and other staff at the Brain Research Imaging Centre, University of Edinburgh; (v) nurses and staff at the WTCRF where the phenotypic data and DNA were collected; (vi) staff at the Lothian Health Board; and (vii) the staff at the SCRE Centre, University of Glasgow (<http://www.gla.ac.uk/schools/education>). The LBC1936 data were collected by a Research Into Ageing program grant; this research continues as part of the Age UK-funded (formerly Help the Aged) Disconnected Mind project. The study is conducted within CCACE, part of the cross council Lifelong Health and Wellbeing Initiative (G0700704/84698). Funding from the BBSRC, EPSRC, ESRC and MRC is gratefully acknowledged. The LBC1936 website is <http://www.lothianbirthcohort.ed.ac.uk>.

References

- 1 Salthouse T. Major Issues in Cognitive Aging. ISBN 9780195372151. Oxford University Press, USA, 2010.
- 2 McGurn B, Deary IJ, Starr JM. Childhood cognitive ability and risk of late-onset Alzheimer and vascular dementia. *Neurology* 2008; **71**: 1051–6.
- 3 Kirkwood TB. Gerontology: healthy old age. *Nature* 2008; **455**:739–40.
- 4 Deary IJ, Penke L, Johnson W. The neuroscience of human intelligence differences. *Nat Rev Neurosci* 2010; **11**:201–11.
- 5 Whalley LJ, Deary IJ, Appleton CL, Starr JM. Cognitive reserve and the neurobiology of cognitive aging. *Ageing Res Rev* 2004; **3**:369–82.
- 6 Ikram MA, Vrooman HA, Vernooij MW *et al.* Brain tissue volumes in relation to cognitive function and risk of dementia. *Neurobiol Aging* 2010; **31**:378–86.
- 7 Farrell C, Chappell F, Armitage PA *et al.* Development and initial testing of normal reference MR images for the brain at ages 65–70 and 75–80 years. *Eur Radiol* 2009; **19**:177–83.
- 8 O'Sullivan M, Jones DK, Summers PE, Morris RG, Williams SC, Markus HS. Evidence for cortical 'disconnection' as a mechanism of age-related cognitive decline. *Neurology* 2001; **57**:632–8.
- 9 Basser PJ, Mattiello J, LeBihan D. Estimation of the effective self-diffusion tensor from the NMR spin echo. *J Magn Reson B* 1994; **103**:247–54.
- 10 Pierpaoli C, Jezzard P, Basser PJ, Barnett A, Di Chiro G. Diffusion tensor MR imaging of the human brain. *Radiology* 1996; **201**: 637–48.
- 11 Basser PJ, Pajevic S, Pierpaoli C, Duda J, Aldroubi A. In vivo fiber tractography using DT-MRI data. *Magn Reson Med* 2000; **44**: 625–32.
- 12 Sullivan EV, Adalsteinsson E, Pfefferbaum A. Selective age-related degradation of anterior callosal fiber bundles quantified in vivo with fiber tracking. *Cereb Cortex* 2006; **16**:1030–9.
- 13 Hsu JL, Van Hecke W, Bai CH *et al.* Microstructural white matter changes in normal aging: a diffusion tensor imaging study with higher-order polynomial regression models. *NeuroImage* 2010; **49**:32–43.
- 14 Salat DH, Tuch DS, Greve DN *et al.* Age-related alterations in white matter microstructure measured by diffusion tensor imaging. *Neurobiol Aging* 2005; **26**:1215–27.
- 15 Pfefferbaum A, Adalsteinsson E, Sullivan EV. Frontal circuitry degradation marks healthy adult aging: evidence from diffusion tensor imaging. *NeuroImage* 2005; **26**:891–9.
- 16 Deary IJ, Bastin ME, Pattie A *et al.* White matter integrity and cognition in childhood and old age. *Neurology* 2006; **66**:505–12.

- 17 Sullivan EV, Rohlfing T, Pfefferbaum A. Quantitative fiber tracking of lateral and interhemispheric white matter systems in normal aging: relations to timed performance. *Neurobiol Aging* 2010; **31**: 464–81.
- 18 Madden DJ, Spaniol J, Costello MC et al. Cerebral white matter integrity mediates adult age differences in cognitive performance. *J Cogn Neurosci* 2009; **21**:289–302.
- 19 Fazekas F, Ropele S, Enzinger C et al. MTI of white matter hyperintensities. *Brain* 2005; **128**:2926–32.
- 20 Silver NC, Barker GJ, MacManus DG, Tofts PS, Miller DH. Magnetisation transfer ratio of normal brain white matter: a normative database spanning four decades of life. *J Neurol Neurosurg Psychiatry* 1997; **62**:223–8.
- 21 Gunning-Dixon FM, Raz N. The cognitive correlates of white matter abnormalities in normal aging: a quantitative review. *Neuropsychology* 2000; **14**:224–32.
- 22 Vermeer SE, Hollander M; Rotterdam Scan Study. et al. Silent brain infarcts and white matter lesions increase stroke risk in the general population: the Rotterdam Scan Study. *Stroke* 2003; **34**:1126–9.
- 23 Deary IJ, Leaper SA, Murray AD, Staff RT, Whalley LJ. Cerebral white matter abnormalities and lifetime cognitive change. A 66-year follow-up of the Scottish Mental Survey of 1932. *Psychol Aging* 2003; **18**:140–8.
- 24 Frisoni GB, Galluzzi S, Pantoni L, Filippi M. The effect of white matter lesions on cognition in the elderly – small but detectable. *Nat Clin Pract Neurol* 2007; **3**:620–7.
- 25 Debette S, Markus HS. The clinical importance of white matter hyperintensities on brain magnetic resonance imaging: systematic review and meta-analysis. *BMJ* 2010; **341**:c3666.
- 26 Bastin ME, Clayden JD, Pattie A, Gerrish IF, Wardlaw JM, Deary IJ. Diffusion tensor and magnetization transfer MRI measurements of periventricular white matter hyperintensities in old age. *Neurobiol Aging* 2009; **30**:125–36.
- 27 Schmidt R, Ropele S; LADIS study group. et al. Diffusion-weighted imaging and cognition in the leukoariosis and disability in the elderly study. *Stroke* 2010; **41**:e402–8.
- 28 Bastin ME, Sinha S, Whittle IR, Wardlaw JM. Measurements of water diffusion and T1 values in peritumoural oedematous brain. *Neuroreport* 2002; **13**:1335–40.
- 29 Leys D, Englund E, Del Ser T et al. White matter changes in stroke patients. Relationship with stroke subtype and outcome. *Eur Neurol* 1999; **42**:67–75.
- 30 Vermeer SE, Longstreth WT, Koudstaal PJ. Silent brain infarcts: a systematic review. *Lancet Neurol* 2007; **6**:611–9.
- 31 Doubal FN, MacLulich AM, Ferguson KJ, Dennis MS, Wardlaw JM. Enlarged perivascular spaces on MRI are a feature of cerebral small vessel disease. *Stroke* 2010; **41**:450–4.
- 32 Cordonnier C, Al-Shahi Salman R, Wardlaw J. Spontaneous brain microbleeds: systematic review, subgroup analyses and standards for study design and reporting. *Brain* 2007; **130**:1988–2003.
- 33 MacLulich AM, Wardlaw JM, Ferguson KJ, Starr JM, Seckl JR, Deary IJ. Enlarged perivascular spaces are associated with cognitive function in healthy elderly men. *J Neurol Neurosurg Psychiatry* 2004; **75**: 1519–23.
- 34 Wardlaw JM, Doubal F, Armitage P et al. Lacunar stroke is associated with diffuse blood–brain barrier dysfunction. *Ann Neurol* 2009; **65**: 194–202.
- 35 Wuerfel J, Haertle M, Waiczies H et al. Perivascular spaces – MRI marker of inflammatory activity in the brain? *Brain* 2008; **131**: 2332–40.
- 36 Schipper HM. Brain iron deposition and the free radical-mitochondrial theory of ageing. *Ageing Res Rev* 2004; **3**:265–301.
- 37 Penke L, Valdés Hernández MC, Maniega SM et al. Brain iron deposits are associated with general cognitive ability and cognitive aging. *Neurobiol Aging* 2010, PMID: 20542597.
- 38 Shenkin SD, Rivers CS, Deary IJ, Starr JM, Wardlaw JM. Maximum (prior) brain size, not atrophy, correlates with cognition in community-dwelling older people: a cross-sectional neuroimaging study. *BMC Geriatr* 2009; **9**:12.
- 39 Shenkin SD, Deary IJ, Starr JM. Birth parameters and cognitive ability in older age: a follow-up study of people born 1921–1926. *Gerontology* 2009; **55**:92–8.
- 40 Shenkin SD, Bastin ME, Macgillivray TJ, Deary IJ, Starr JM, Wardlaw JM. Birth parameters are associated with late-life white matter integrity in community-dwelling older people. *Stroke* 2009; **40**:1225–8.
- 41 Deary IJ, Johnson W, Houlihan LM. Genetic foundations of human intelligence. *Hum Genet* 2009; **126**:215–32.
- 42 Houlihan LM, Harris SE, Luciano M et al. Replication study of candidate genes for cognitive abilities: the Lothian Birth Cohort 1936. *Genes Brain Behav* 2009; **8**:238–47.
- 43 Deary IJ, Johnson W. Intelligence and education: causal perceptions drive analytic processes and therefore conclusions. *Int J Epidemiol* 2010; **39**:1362–9.
- 44 Lawlor DA, Batty GD, Morton SM et al. Early life predictors of childhood intelligence: evidence from the Aberdeen children of the 1950s study. *J Epidemiol Community Health* 2005; **59**:656–63.
- 45 Richards M, Deary IJ. A life course approach to cognitive reserve: a model for cognitive aging and development? *Ann Neurol* 2005; **58**: 617–22.
- 46 Singhal A, Cole TJ, Lucas A. Early nutrition in preterm infants and later blood pressure: two cohorts after randomised trials. *Lancet* 2001; **357**:413–9.
- 47 Prins ND, van Dijk EJ, den Heijer T et al. Cerebral small-vessel disease and decline in information processing speed, executive function and memory. *Brain* 2005; **128**:2034–41.
- 48 Longstreth WT, Arnold AM, Beauchamp NJ, et al. Incidence, manifestations, and predictors of worsening white matter on serial cranial magnetic resonance imaging in the elderly: the Cardiovascular Health Study. *Stroke* 2005; **36**:56–61.
- 49 Gouw AA, van der Flier WM; LADIS study group et al. On the etiology of incident brain lacunes: longitudinal observations from the LADIS study. *Stroke* 2008; **39**:3083–5.
- 50 Knoops AJ, van der Graaf Y, Appelman AP, Mali WP, Geerlings MI. Total cerebral blood flow and hippocampal volume in patients with arterial disease. The SMART-MR study. *J Cereb Blood Flow Metab* 2009; **29**:1727–33.
- 51 van Norden AG, Fick WF, de Laat KF et al. Subjective cognitive failures and hippocampal volume in elderly with white matter lesions. *Neurology* 2008; **71**:1152–9.
- 52 Deary IJ, Whalley LJ, Starr JM. A Lifetime of Intelligence: Follow-Up Studies of the Scottish Mental Surveys of 1932 and 1947. ISBN 9781433804007. American Psychological Association, Washington, USA, 2009.
- 53 Deary IJ, Gow AJ, Taylor MD et al. The Lothian Birth Cohort 1936: a study to examine influences on cognitive ageing from age 11 to age 70 and beyond. *BMC Geriatr* 2007; **7**:28.
- 54 Jones DK, Williams SC, Gasston D, Horsfield MA, Simmons A, Howard R. Isotropic resolution diffusion tensor imaging with whole brain acquisition in a clinically acceptable time. *Hum Brain Mapp* 2002; **15**:216–30.
- 55 Morris Z, Whiteley WN, Longstreth WT Jr et al. Incidental findings on brain magnetic resonance imaging: systematic review and meta-analysis. *BMJ* 2009; **339**:b3016.
- 56 Alexandrov A. Cerebral vessels; in Zwiebel WJ, Pellerito JS (eds): Introduction to Vascular Sonography. ISBN 0721606318, 5th edn. Philadelphia: Elsevier Saunders, 2005: 107–31.
- 57 Lammie GA, Wardlaw J, Allan P, Ruckley CV, Peek R, Signorini DF. What pathological components indicate carotid atheroma activity and can these be identified reliably using ultrasound? *Eur J Ultrasound* 2000; **11**:77–86.

- 58 Wardlaw JM, Lewis S. Carotid stenosis measurement on colour Doppler ultrasound: agreement of ECST, NASCET and CCA methods applied to ultrasound with intra-arterial angiographic stenosis measurement. *Eur J Radiol* 2005; **56**:205–11.
- 59 Haller C, Schulz J, Schmidt-Trucksäss A *et al.* Sequential based analysis of intima-media thickness (IMT) in common carotid artery studies. *Atherosclerosis* 2007; **195**:e203–9.
- 60 Lorenz MW, Markus HS, Bots ML, Rosvall M, Sitzer M. Prediction of clinical cardiovascular events with carotid intima-media thickness: a systematic review and meta-analysis. *Circulation* 2007; **115**:459–67.
- 61 Simons PC, Algra A, Bots ML, Grobbee DE, van der Graaf Y. Common carotid intima-media thickness and arterial stiffness: indicators of cardiovascular risk in high-risk patients. The SMART Study (Second Manifestations of ARterial disease). *Circulation* 1999; **100**:951–7.
- 62 Shenkin SD, Bastin ME, MacGillivray TJ *et al.* Carotid intima-media thickness and cerebrovascular disease in community-dwelling older people without stroke. *Stroke* 2010; **41**:2083–6.
- 63 Wardlaw JM, Ferguson KJ, Graham C. White matter hyperintensities and rating scales—observer reliability varies with lesion load. *J Neurol* 2004; **251**:584–90.
- 64 Fazekas F, Chawluk JB, Alavi A, Hurtig HI, Zimmerman RA. MR signal abnormalities at 1.5 T in Alzheimer's dementia and normal aging. *Am J Roentgenol* 1987; **149**:351–6.
- 65 Wahlund LO, Barkhof F; European Task Force on Age-Related White Matter Changes *et al.* A new rating scale for age-related white matter changes applicable to MRI and CT. *Stroke* 2001; **32**:1318–22.
- 66 Bocti C, Swartz RH, Gao FQ, Sahlas DJ, Behl P, Black SE. A new visual rating scale to assess strategic white matter hyperintensities within cholinergic pathways in dementia. *Stroke* 2005; **36**:2126–31.
- 67 Wardlaw JM. Is it an infarct or a haemorrhage?; in Warlow CP, van Gijn J, Dennis MS, Wardlaw JM, Bamford J, Hankey G, Sandercock PAG, Rinkel G, Langhorne P, Sudlow C, Rothwell P (eds): *Stroke. Practical Management*. ISBN 9781405127660, 3rd edn. Oxford: Blackwell Scientific Ltd, 2008, pp 181–258.
- 68 Wardlaw JM, Sellar R. A simple practical classification of cerebral infarcts on CT and its interobserver reliability. *Am J Neuroradiol* 1994; **15**:1933–9.
- 69 Potter GM, Doubal FN, Jackson CA *et al.* Counting cavitating lacunes underestimates the burden of lacunar infarction. *Stroke* 2010; **41**:267–72.
- 70 Cordonnier C, Potter GM, Jackson CA *et al.* Improving interrater agreement about brain microbleeds: development of the Brain Observer MicroBleed Scale (BOMBS). *Stroke* 2009; **40**:94–9.
- 71 Casanova ME, Araque JM. Mineralization of the basal ganglia: implications for neuropsychiatry, pathology and neuroimaging. *Psychiatry Res* 2003; **121**:59–87.
- 72 Payne ME, Fetzter DL, MacFall JR, Provenzale JM, Byrum CE, Krishnan KR. Development of a semi-automated method for quantification of MRI gray and white matter lesions in geriatric subjects. *Psychiatry Res* 2002; **115**:63–77.
- 73 Vintners HV, Mah VH. Vascular diseases; in Duckett S (ed): *The Pathology of the Aging Human Nervous System*. ISBN 9780812113556. Philadelphia: Lippincott, Williams and Wilkins, 1991: 41–4.
- 74 Valdés Hernandez MC, Ferguson KJ, Chappell FM, Wardlaw JM. New multispectral MRI data fusion technique for white matter lesion segmentation: method and comparison with thresholding in FLAIR images. *Eur Radiol* 2010; **20**:1684–91.
- 75 Floyd RW, Steinberg L. An adaptive algorithm for spatial grey scale. *Proc Soc Inform Display* 1976; **17**:75–7.
- 76 Jenkinson M, Smith S. A global optimisation method for robust affine registration of brain images. *Med Image Anal* 2001; **5**:143–56.
- 77 Smith SM. Fast robust automated brain extraction. *Hum Brain Mapp* 2002; **17**:143–55.
- 78 Behrens TE, Berg HJ, Jbabdi S, Rushworth MF, Woolrich MW. Probabilistic diffusion tractography with multiple fibre orientations: what can we gain. *NeuroImage* 2007; **34**:144–55.
- 79 Armitage PA, Schwindack C, Bastin ME, Whittle IR. Quantitative assessment of intracranial tumor response to dexamethasone using diffusion, perfusion and permeability magnetic resonance imaging. *Magn Reson Imaging* 2007; **25**:303–10.
- 80 Clayden JD, Storkey AJ, Bastin ME. A probabilistic model-based approach to consistent white matter tract segmentation. *IEEE Trans Med Imaging* 2007; **26**:1555–61.
- 81 Clayden JD, Storkey AJ, Muñoz Maniega S, Bastin ME. Reproducibility of tract segmentation between sessions using an unsupervised modelling-based approach. *NeuroImage* 2009; **45**:377–85.
- 82 Bastin ME, Muñoz Maniega S, Ferguson KJ *et al.* Quantifying the effects of normal ageing on white matter structure using unsupervised tract shape modelling. *NeuroImage* 2010; **51**:1–10.
- 83 Penke L, Muñoz Maniega S, Murray C *et al.* A general factor of brain white matter integrity predicts information processing speed in healthy older people. *J Neurosci* 2010; **30**:7569–74.
- 84 Corley J, Jia X, Kyle JA *et al.* Caffeine consumption and cognitive function at age 70: the Lothian Birth Cohort 1936 study. *Psychosom Med* 2010; **72**:206–14.
- 85 Penke L, Muñoz Maniega S, Houlihan LM *et al.* White matter integrity in the splenium of the corpus callosum is related to successful cognitive aging and partly mediates the protective effect of an ancestral polymorphism in ADRB2. *Behav Genet* 2010; **40**:146–56.
- 86 Valdés Hernandez M, Penke L, Muñoz Maniega S *et al.* White matter lesion intensity and cognitive ability: relationships in youth and old age. Joint annual meeting of ISMRM and ESMRMB. *Proc ISMRM* 2010; **18**:2001.
- 87 Ikram MA, Vernooij MW, Vrooman HA, Hofman A, Breteler MM. Brain tissue volumes and small vessel disease in relation to the risk of mortality. *Neurobiol Aging* 2009; **30**:450–6.
- 88 de Leeuw FE, Barkhof F, Scheltens P. White matter lesions and hippocampal atrophy in Alzheimer's disease. *Neurology* 2004; **62**:310–2.